IOPscience iopscience.iop.org

Home Search Collections Journals About Contact us My IOPscience

Structural characterization of ZnO thin films grown on various substrates by pulsed laser deposition

This article has been downloaded from IOPscience. Please scroll down to see the full text article.

2012 J. Phys. D: Appl. Phys. 45 225101

(http://iopscience.iop.org/0022-3727/45/22/225101)

View the table of contents for this issue, or go to the journal homepage for more

Download details:
IP Address: 195.113.24.181
The article was downloaded on 19/09/2012 at 10:53

Please note that terms and conditions apply.

J. Phys. D: Appl. Phys. **45** (2012) 225101 (12pp) doi:10.1088/0022-3727/45/22/225101

Structural characterization of ZnO thin films grown on various substrates by pulsed laser deposition

M Novotný[1], J Čížek[2], R Kužel[2], J Bulíř[1], J Lančok[1], J Connolly[3], E McCarthy[3], S Krishnamurthy[3], J-P Mosnier[3], W Anwand[4] and G Brauer[4]

[1] Institute of Physics, Academy of Sciences of the Czech Republic, Na Slovance 2, 182 21 Prague, Czech Republic
[2] Faculty of Mathematics and Physics, Charles University in Prague, 121 16 Prague 2, Czech Republic
[3] National Centre for Plasma Science and Technology, School of Physical Sciences, Glasnevin, Dublin 9, Ireland
[4] Institut für Strahlenphysik, Forschungszentrum Dresden-Rossendorf, PO Box 510 119, D-01314 Dresden, Germany

Received 16 February 2012, in final form 9 April 2012
Published 16 May 2012
Online at stacks.iop.org/JPhysD/45/225101

Abstract
ZnO thin films were grown by pulsed laser deposition on three different substrates: sapphire (0 0 0 1), MgO (1 0 0) and fused silica (FS). The structure and morphology of the films were characterized by x-ray diffraction and scanning electron microscopy and defect studies were carried out using slow positron implantation spectroscopy (SPIS). Films deposited on all substrates studied in this work exhibit the wurtzite ZnO structure and are characterized by an average crystallite size of 20–100 nm. However, strong differences in the microstructure of films deposited on various substrates were found. The ZnO films deposited on MgO and sapphire single-crystalline substrates exhibit local epitaxy, i.e. a well-defined relation between film crystallites and the substrate. Domains with different orientation relationships with the substrate were found in both films. On the other hand, the film deposited on the FS substrate exhibits fibre texture with random lateral orientation of crystallites. Extremely high compressive in-plane stress of $\sigma \sim 14$ GPa was determined in the film deposited on the MgO substrate, while the film deposited on sapphire is virtually stress-free, and the film deposited on the FS substrate exhibits a tensile in-plane stress of $\sigma \sim 0.9$ GPa. SPIS investigations revealed that the concentration of open-volume defects in the ZnO films is substantially higher than that in a bulk ZnO single crystal. Moreover, the ZnO films deposited on MgO and sapphire single-crystalline substrates exhibit a significantly higher density of defects than the film deposited on the amorphous FS substrate.

(Some figures may appear in colour only in the online journal)

1. Introduction

Externally pumped lasing observed in epitaxial ZnO films stimulated a great interest in the preparation of high-quality ZnO films for realizing efficient excitonic UV blue lasers at room temperature [1, 2]. Moreover, ZnO films are considered as promising materials for flat panel displays and optical coatings for solar cells [3]. ZnO films can be fabricated by several techniques, e.g. dip coating, sol–gel [4], magnetron sputtering [5, 6] or pulsed laser deposition (PLD) [7–15].

PLD enables the production of high-quality ZnO films at lower temperatures than other methods due to the high energy of ablated particles in the laser-produced plasma plume [12, 13]. There are several important parameters which determine the morphology and microstructure of thin films deposited by PLD: (i) the energy and surface dynamics of

 © 2012 IOP Publishing Ltd Printed in the UK & the USA

adsorbed atoms, determined mainly by the laser wavelength, fluence and substrate temperature, (ii) the ambient atmosphere in the deposition chamber and (iii) the type of substrate. Previous works have explored aspects of the relationship between the thin film properties and these growth parameters. Cracium *et al* [14] used PLD for deposition of ZnO films on glass and silicon substrates and studied the influence of deposition parameters on the film quality. The best films were obtained using laser fluences around $2\,\mathrm{J\,cm^{-2}}$ and the substrate temperature T_s between 300 and 350 °C. Systematic investigations of ZnO films deposited by PLD on sapphire (0 0 0 1) were performed in [15]. ZnO films were grown at 750 °C under various oxygen background pressures. All ZnO layers were found to be *c*-axis oriented; however, the in-plane orientation was strongly influenced by the oxygen pressure [15]. The morphology of ZnO films deposited at low oxygen pressures (10^{-3}–10^{-2} Pa) exhibited 3D growth features evidenced by well-faceted hexagons. Increasing the oxygen pressure to ~1 Pa led to a substantial reduction in roughness, and the consequent formation of smooth films. A further increase in oxygen pressure to 10 Pa resulted in hetero-epitaxial growth of films exhibiting irregular grains with different sizes [15].

The majority of ZnO films investigated to date have been of thicknesses of several hundred nm. Very thin ZnO films (thickness below 100 nm), i.e. much less than the wavelength of visible light, are becoming increasingly important in nanotechnology applications nowadays, in particular in those involving quantum confinement effects [7]. It is well known that with decreasing film thickness the role of surface energy and the energy of the interface between the film and the substrate becomes increasingly important. As a consequence very thin films may exhibit extraordinary structures and/or orientation with the substrate. Suchea *et al* [8] showed that very thin (40 nm) ZnO films, grown on glass substrates at various substrate temperatures, exhibited granular morphology and polycrystalline structure. Nie *et al* [7] and Myong *et al* [11] studied the structural and optical properties of very thin ZnO films grown on a sapphire (0 0 0 1) substrate and found that the band-gap energy increased with decreasing film thickness and decreasing out-of-plane crystallite size, respectively [7, 11] due to the quantum confinement effect.

In this work, we aim to further clarify the role played by the substrate on the properties of very thin ZnO films. To this end, we have carried out systematic investigation of the structure, morphology and defect properties of very thin ($\leqslant$80 nm thickness) ZnO films, deposited by PLD under identical conditions, on MgO (1 0 0), sapphire (0 0 0 1) and fused silica (FS) substrates, respectively. We selected these substrates because of their different crystallographic structures; MgO crystallizes in a rocksalt structure in contrast to the hexagonal lattice of sapphire and amorphous phase of FS. The substrates' properties make them interesting for ZnO growth study [16, 17]. Structural and morphological characterizations of the films were performed using x-ray diffraction (XRD) combined with scanning electron microscopy (SEM) and measurement of optical transmittance and reflectance. Since lattice defects strongly influence the electrical and optical properties of ZnO films, slow positron implantation spectroscopy (SPIS) [18] was employed for characterization of open-volume defects in the ZnO films.

In the rest of the paper, we present detailed analyses of the experimental results and discuss the marked differences that were observed in the properties of the thin ZnO films as a function of the type of substrate.

2. Experimental details

2.1. Samples

The experiments were carried out in a stainless-steel vacuum chamber (dedicated to ZnO growth) evacuated by oil-free turbomolecular pumping to a base pressure of 2×10^{-4} Pa. A frequency-quadrupled Nd : YAG laser providing 90 mJ of 266 nm laser light in a 6 ns pulse was used to ablate an ultra-high-purity ZnO ceramic target with a fluence of $2.8\,\mathrm{J\,cm^{-2}}$ on the target. The laser was always operated at the repetition rate of 10 Hz and all the samples were grown as a result of 5200 laser shots. The target-to-substrate distance was kept fixed at 55 mm in all the experiments. The films were grown in oxygen atmosphere at a pressure of 10 Pa (5N-pure oxygen flow rate was 40 sccm). These conditions were optimized in our previous works [19, 20] as favourable for ZnO p-type doping in order to avoid compensation due to oxygen vacancies. Polished sapphire (0 0 0 1), MgO (1 0 0) and FS supplied by MaTecK GmbH were used as substrates for the depositions. After standard cleaning and degreasing, all substrates were baked out in vacuum at 950 °C for 5 min (temperature rise/drop ramps were 30 min) before the deposition in order to remove remaining surface contamination. The ZnO thin films were grown at a substrate temperature of $T_s = 300$ °C and subsequently annealed *in situ* at 750 °C (temperature rise and drop ramp were 15 min and 60 min, respectively) in a 10 Pa oxygen atmosphere.

A hydrothermally grown bulk ZnO (0 0 0 1) single crystal with O-terminated surface supplied by MaTecK GmbH was used as a reference material in SPIS investigations.

2.2. Characterization of optical properties

The optical transmittance and reflectance of the samples were both measured in the wavelength range from 250 to 900 nm using an apparatus coupled to a spectrophotometer (USB4000, Ocean Optics) by means of optical fibres. Absolute transmittance and reflectance were obtained using the standard reduction procedures of the optical transmission and reflection measurements, based on dark background subtraction and normalization of intensity with respect to void sample intensity and the use of a known reflective standard (aluminium mirror), respectively.

2.3. SEM

The morphology of the samples was observed using a scanning electron microscope, JEOL JSM-7500F.

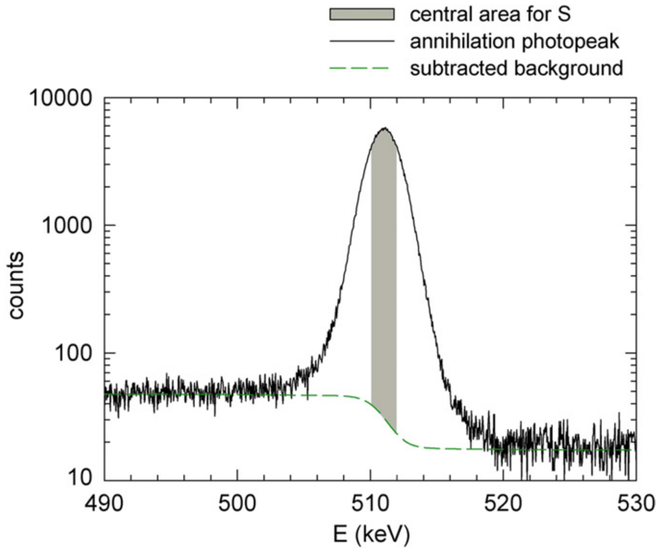

Figure 1. An example of Doppler broadened annihilation photopeak measured on the ZnO film deposited on the FS substrate using positrons with an energy of 2 keV. Dashed line shows subtracted background. The shadowed region shows the central area of the annihilation photopeak used for calculation of the *S* parameter.

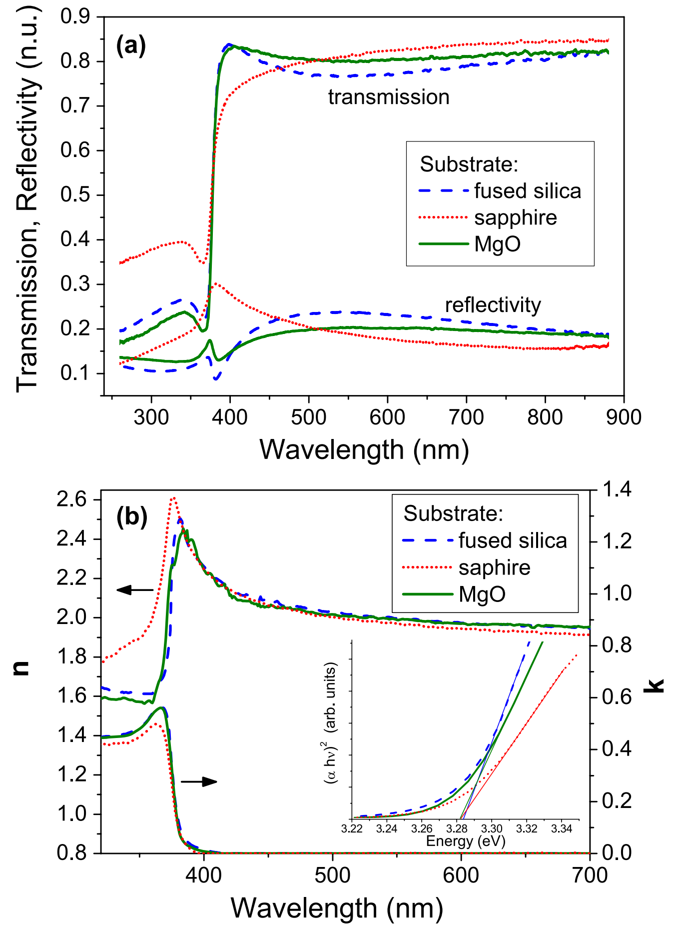

Figure 2. (*a*) Optical reflectivity and transmission spectra measured on ZnO films deposited on the sapphire (0 0 0 1), MgO (1 0 0) and FS substrates; (*b*) Refractive index *n*, extinction coefficient *k* and Tauc's plots for ZnO films deposited on the sapphire (0 0 0 1), MgO (1 0 0) and FS substrates.

2.4. XRD

The crystalline structure of the ZnO films was investigated using X'Pert Pro and X'Pert MRD powder diffractometers (PANalytical B.V) with Cu K$\alpha_{1,2}$ radiation (wavelength 1.540 562 Å) in conventional para-focusing Bragg–Brentano (Θ–2Θ) geometry with automatic divergence and anti-scatter slits and grazing incidence ($\Theta = 0.35°$ and $\Theta = 0.5°$) parallel beam arrangement with a Goebel mirror. The X'Pert MRD diffractometer equipped with a polycapillary and Eulerian cradle was used for texture characterization and all measurements of asymmetric reflections.

2.5. SPIS

SPIS investigations were performed using a magnetically guided slow positron beam SPONSOR [21]. The energy of positrons in the beam can be varied in the range from 0.03 to 36 keV. The implantation profile of positrons with energy E is described by the Makhovian function [22] and the mean positron penetration depth z_{mean} (expressed in Å) increases with energy following the power law [23, 24]

$$z_{\mathrm{mean}} = \frac{400}{\rho} E^{1.6}, \tag{1}$$

where ρ is the sample density in g cm^{-3} and E is expressed in keV [23, 24]. Using equation (1) and ZnO density of 5.606 g cm^{-3} one can calculate that the mean positron penetration depths into ZnO are 0.026 nm and 2205 nm for positron energies of 0.03 keV and 36 keV, respectively.

The non-zero momentum of an annihilating pair causes Doppler broadening (DB) of the annihilation photopeak which was measured using a HPGe detector with an energy resolution of (1.09 ± 0.01) keV at 511 keV, i.e. at the position of the annihilation photopeak. An example of Doppler broadened annihilation photopeak is shown in figure 1. The evaluation of DB was performed using the line shape S parameter [18, 25] calculated as the central area of the annihilation photopeak (with subtracted background) divided by the net peak area. Hence, the S parameter is a measure of the contribution of positrons annihilated by low-momentum electrons. The central energy region shown in figure 1 was selected from 510.07 to 511.93 keV so that the bulk S parameter value for the reference ZnO crystal S_0 is close to 0.5, where the S parameter is most sensitive to changes in the shape of the annihilation photopeak. All the S parameters presented in this paper are normalized to the bulk S parameter for the reference ZnO crystal $S_0 = 0.5068(5)$. The dependence of the S parameter on positron energy E was analysed using the VEPFIT software package [26].

3. Results and discussion

3.1. Optical properties

The measured reflectance (R) and transmittance (T) spectra are shown in figure 2(*a*). The spectra were carefully analysed in the framework of a numerical model based on the solution of the Fresnel equations for the ambient/substrate/ZnO

Table 1. Properties of ZnO films deposited on MgO (1 0 0), sapphire (0 0 0 1) and FS substrates: the band-gap energy derived from Tauc's plot ($E_{g,Tauc}$) and exciton position ($E_{g,exc}$), the film thickness calculated from measurement of optical reflectance and transmittance (t_{OPT}), determined from XRD reflectivity curves (t_{XRD}) and estimated by SPIS (t_{SPIS}); the mean crystallite size estimated by SEM (d_{SEM}); the lattice parameters a, c determined by XRD, the stress σ determined by XRD; the S parameter for the ZnO layer S_{ZnO}; the mean positron diffusion length L_+ and the surface value of the S parameter S_{surf}. Errors expressed in the order of the last significant digit are shown in parentheses.

Substrate	MgO (1 0 0)	Sapphire (0 0 0 1)	Fused silica
$E_{g,Tauc}$ (eV)	3.28(5)	3.28(5)	3.28(5)
$E_{g,exc}$ (eV)	3.38(1)	3.41(1)	3.38(1)
t_{OPT} (nm)	81(3)	41(3)	75(3)
t_{XRD} (nm)	76(2)	48(2)	75(2)
t_{SPIS} (nm)	80(2)	45(3)	76(1)
d_{SEM} (nm)	30–100	25–70	20–50
a (nm)	0.3249(1)	0.3258(1)	0.325 69(7)
c (nm)	0.520 87(3)	0.5207(7)	0.5195(2)
σ (GPa)	14(2)	≈0	0.9(1)
S_{ZnO}	1.0566(6)	1.0552(8)	1.027(1)
L_+ (nm)	4.9(2)	6.9(1)	21.0(4)
S_{surf}	1.137(8)	1.184(8)	1.176(8)

film/ambient layered structure. The data were first analysed in the transparent region using a simple Cauchy dispersion function for the ZnO layer by fitting the model with the measured R, T spectra. This procedure allowed us to obtain estimates for the film thicknesses t_{OPT}, which are displayed in table 1. The estimated thicknesses were 81 nm, 41 nm and 75 nm for MgO, sapphire and fused silica substrates, respectively. Such thin transparent layers do not induce multiple interference oscillations in the measured range. Thus, the accuracy of the thickness estimation is slightly lowered leading to an estimation error of a few nm. The estimated thickness is used in the fitting procedure in the absorbing region of the spectra. The films deposited on MgO and FS both exhibit comparable thickness, but the film deposited on sapphire is remarkably thinner despite the fact that all parameters which are under control were kept unchanged. It could be caused by the fact that the ZnO film on sapphire grows in an orientation which differs from the other films, see section 3.3. Moreover, the lower thickness of the film on the sapphire substrate might also be caused by the target degradation during its laser ablation.

The refractive index (n) and the extinction coefficient (k) in the absorbing region were evaluated by a fitting procedure of R, T data independently from the dispersion model of the ZnO layer by processing them for each wavelength separately. As the thin ZnO films were partially transparent, even in the absorbing region, unambiguous evaluation of both the refractive indices and extinction coefficients was possible. The results are shown in figure 2(b). The $n(\lambda)$ curves for the ZnO films deposited on MgO and FS substrates are almost identical, whereas that for ZnO on the sapphire substrate shows a slightly lower refractive index in the transparent region. The values of the linear absorption coefficient obtained from the k values near the absorption edge were used to estimate the energy of the (direct) optical band gap E_g of the ZnO thin films. Tauc's plot method was used whereby E_g is estimated from a linear extrapolation of the dependence of the square of the absorption on the photon energy (inset of figure 2(b)). A value of $E_{g,Tauc} = (3.28 \pm 0.05)$ eV was obtained for all the films regardless of the substrate type. This value agrees well with $E_g = 3.26$ eV measured in ZnO films by several authors [7, 27–29], by the method of absorption edge extrapolation (Tauc's plot), but it is significantly smaller than 3.37 eV known for a bulk ZnO crystal at room temperature [30–32]. The lower $E_{g,Tauc}$ value in ZnO films can be attributed to the effects associated with exciton formation which are responsible for significant peak maxima of both $n(\lambda)$ and $k(\lambda)$ curves in the spectral region near the absorption edge. The Coulombic interactions between electrons and holes have a strong influence on the absorption spectrum, which prevents accurate estimation of the band-gap energy from extrapolation of absorption edge [33]. Thus, the correct value of the band-gap energy ($E_{g,exc}$) was estimated from the exciton peak in the absorption spectra, and is shown in table 1. We estimated the band-gap energy of ZnO deposited on MgO and fused silica substrates as equal to $E_{g,exc} = (3.38 \pm 0.01)$ eV, which is close to that of single-crystal ZnO [30–32]. In contrast, the band-gap energy of ZnO deposited on the sapphire substrate was found to be increased being $E_{g,exc} = (3.41 \pm 0.01)$ eV. This slight increase in the band-gap energy is comparable to that measured by Nie *et al* [7] for a 40 nm thick ZnO film on sapphire where it is explained by the quantum confinement effect due to small film thickness and reduction in the mean grain size dimension. However, taking into the account the crystallite size around 25–70 nm, which is much larger than the exciton Bohr radius (about 2 nm in ZnO), significant confinement effects are unlikely to be expected [34, 35]. Hence, the band-gap energy shift for the ZnO film on sapphire might be rather related to its different orientation of growth compared with MgO and FS substrates, i.e. in non-basal orientation with c-planes of ZnO inclined with respect to c-planes of sapphire, as we further discuss in section 3.3.

3.2. Morphology

The morphology of the deposited thin ZnO films was analysed by SEM. The SEM micrographs of the films on FS, sapphire (0 0 0 1) and MgO (1 0 0) substrates are presented in figures 3(a), (b) and (c), respectively, and show nanostructured surface morphologies for all the samples. Similar features in the form of nanocrystalline grains can be distinguished in figures 3(a) and (b) corresponding to the films grown on the FS and sapphire substrates with crystallite sizes lying in the range 20–50 nm and 25–70 nm, respectively. Contrary to our observation a smooth surface with several islands (indicating the film growth in layer-plus-island mode) was reported for the ZnO film of similar thickness on sapphire [11]. However, the film was prepared using a Nd : YAG laser ($\lambda = 355$ nm) at an oxygen pressure of 47 Pa [11]. Different morphologies may be attributed to the higher pressure because the roughness of the ZnO films is found to increase with decreasing oxygen pressure and the films tend to grow rather in 3D mode at a lower pressure [15]; also, the effect of different laser wavelengths

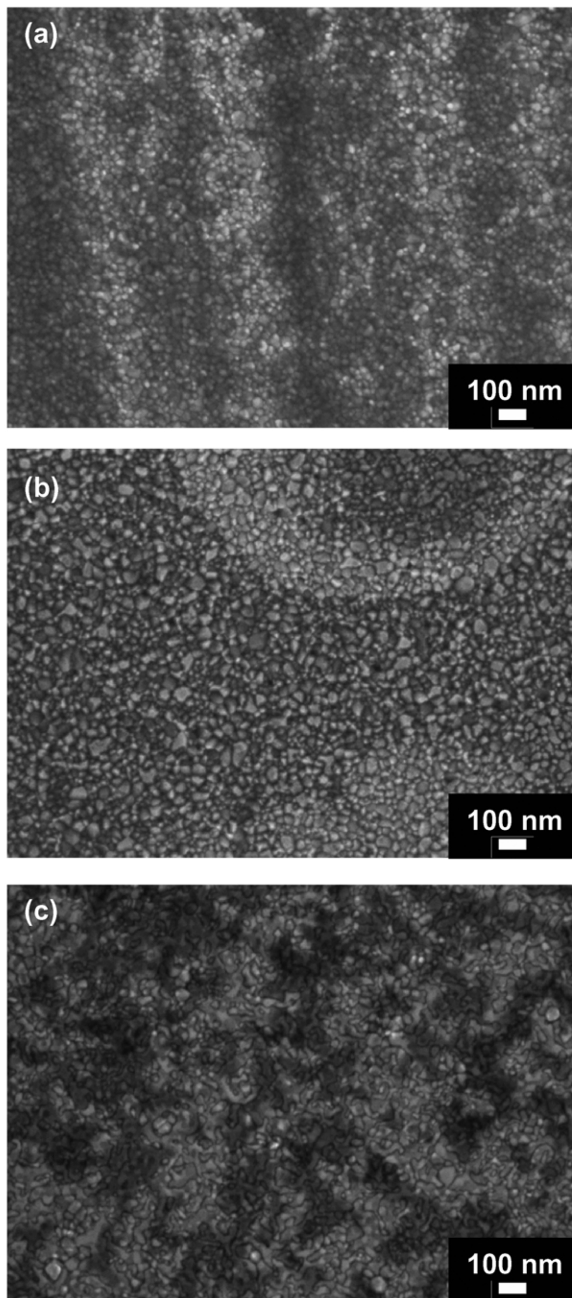

Figure 3. SEM micrographs of ZnO film deposited on the (*a*) FS, (*b*) sapphire (0 0 0 1) and (*c*) MgO (1 0 0) substrates.

cannot be excluded [36, 37]. The mean size distribution of the crystallites appears more homogeneous in the ZnO films grown on the FS substrate, which may be related to the (0 0 0 1) fibre texture (see section 3.3.) leading to completely random lateral orientation of the crystallites in the plane of the FS substrate observed by XRD. A similar morphology was also observed for the ZnO film deposited under congruent conditions on a glass substrate [38].

The film deposited on the MgO (1 0 0) substrate, shown in figure 3(*c*), exhibits a comparatively different morphology in the form of irregularly shaped features. This is attributable to the cubic lattice of the MgO crystal. The crystallite size falls into the interval from 30 to 100 nm. Similar surface features were observed in ZnO films fabricated by ultrasonic spray pyrolysis on MgO substrates at $T_s = 300\,^\circ$C, where nanoparticles merged to form smoother, more compact aggregates [39].

3.3. Structural properties

Film thicknesses t_{XRD} were determined by x-ray reflectivity measurements. The results are listed in table 1 and agree well with those obtained from the optical measurements presented in section 3.1.

Figure 4 shows the XRD patterns taken in grazing incidence parallel beam geometry (angle of incidence $\gamma = 0.35^\circ$) for the ZnO films deposited on the MgO (1 0 0), sapphire (0 0 0 1) and FS substrates. The 0 0 2 diffraction peak is clearly visible in the XRD patterns for all the films while another significant peak is 1 0 3. Note that 4-index ($h\,k\,i\,l$) notation is used for hexagonal lattice planes while 3-index $h\,k\,l$ notation is used for diffraction indices since this is the common nomenclature in the diffraction literature. In the parallel beam grazing incidence geometry, different peaks correspond to the lattice planes differently inclined to the surface (by an angle $\psi = \Theta - \gamma$). Therefore, the 0 0 2 peaks correspond to the (0 0 0 2) (parallel to the (0 0 0 1)) ZnO planes making an angle of about 17° with the surface.

Symmetric Bragg–Brentano scans were also acquired. The one obtained for the film deposited on the FS substrate is also shown in figure 4 as an example. The strong 0 0 2 peak obtained in this geometry reveals a strong (0 0 0 1) preferred grain orientation in the ZnO film deposited on the FS substrate. A strong (0 0 0 1) preferred grain orientation was also found in the ZnO film deposited on the MgO substrate. On the other hand, the 0 0 2 peak was not visible in the symmetric Bragg–Brentano scan performed on the film deposited on the sapphire substrate (not shown here), indicating that this film does not exhibit (0 0 0 1) preferred grain orientation.

Figure 5(*a*) shows a part of the 1 0 1 pole figure for the ZnO film deposited on the FS substrate. The pole figure shows complete cylindrical symmetry, which indicates a fibre (0 0 0 1) texture. Hence, the ZnO film grows on FS with the basal plane parallel to the substrate surface while the lateral orientation of the crystallites is completely random.

On the other hand, the ZnO film deposited on the MgO (1 0 0) substrate exhibits a strong orientation of the grains and local expitaxy which is demonstrated by the 1 0 2 pole figure shown in figure 5(*b*). Azimuthal angle scans (Φ-scans) taken for several asymmetric diffraction planes revealed a pattern of clear periodic maxima. A total of 12 maxima were found for the (h 0 $-h$ l) planes, while for the ($h\,k\,i\,l$) planes this number is 24. This is double the number of peaks that would be expected from the consideration of point symmetry alone and can be understood in terms of two possible orientations, rotated by 30° with respect to each other, of the wurtzite ZnO basal plane on the (1 0 0) MgO cubic lattice plane, see figure 6. Hence, it can be concluded that there are two kinds of rotational domains for the present ZnO films grown on the MgO (1 0 0) substrate. This orientation is also supported by azimuthal angle scans for (1 1 1) lattice planes for the MgO substrate, which exhibit four-fold symmetry and the positions of the MgO 1 1 1 peaks coincide with that of the ZnO $h\,0\,l$ peaks.

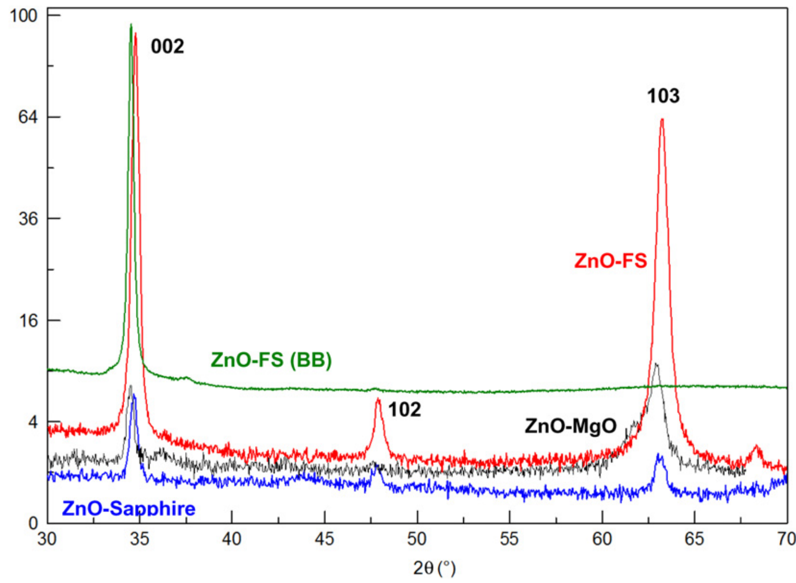

Figure 4. XRD patterns (intensity in counts per second, square-root scale) of ZnO films deposited on sapphire (0 0 0 1) (ZnO-sapphire: bottom thick blue curve), MgO (1 0 0) (ZnO-MgO: thin black curve) and FS (ZnO-FS: upper thick red curve). The patterns were taken in the parallel glancing-angle geometry with the angle of incidence $\gamma = 0.35^\circ$. For comparison, symmetric Bragg–Brentano θ–2θ scan of the ZnO film on FS substrate is shown (ZnO-FS (BB): upper thick green curve).

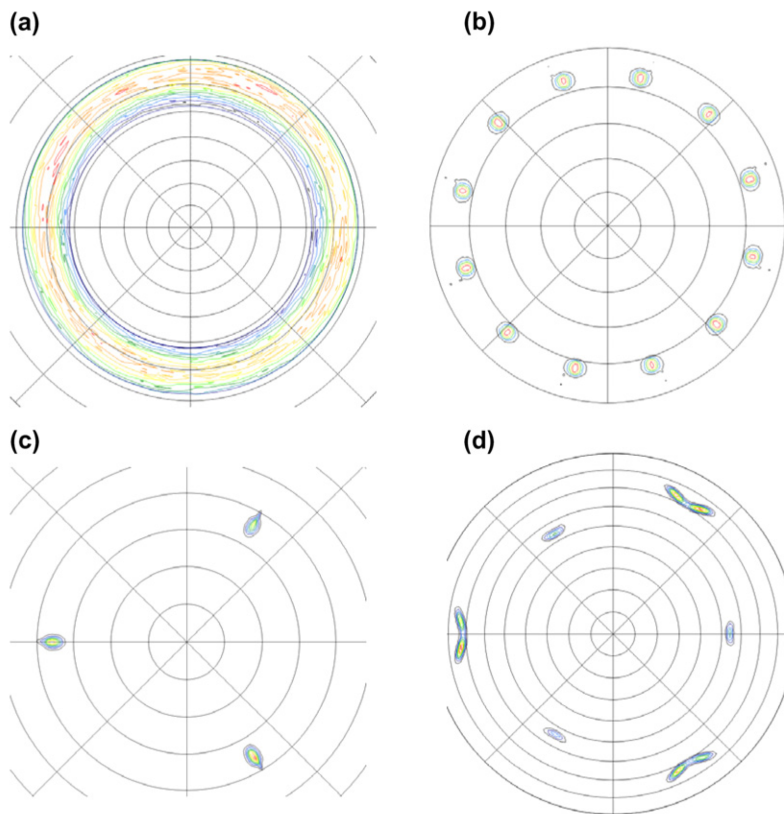

Figure 5. Results of texture measurements: (*a*) part of the 1 0 1 pole figure measured on the ZnO film deposited on the FS substrate (axis divided by $45^\circ - \varphi$, $10^\circ - \psi$); (*b*) 1 0 2 pole figure measured on the ZnO film deposited on the MgO substrate (axis divided by $45^\circ - \varphi$, $18^\circ - \psi$); (*c*) part of the pole figure for 0 0 2 reflection measured on the ZnO film deposited on the sapphire substrate (axis divided by $45^\circ - \varphi$, $10^\circ - \psi$); (*d*) pole figure for 1 0 1 reflection measured on the ZnO film deposited on the sapphire susbtrate (axis divided by $45^\circ - \varphi$, $10^\circ - \psi$).

Texture measurements were also performed on the ZnO film deposited on the sapphire substrate. Figure 5(*c*) shows a part of the pole figure measured on the 0 0 2 reflection which exhibits three-fold symmetry and reveals three clear non-symmetrical maxima at $\psi \sim 36^\circ$. This testifies that the ZnO (0 0 0 1) planes in the ZnO film deposited on sapphire are not parallel to the (0 0 0 1) sapphire surface but are inclined with respect to it by an angle of $\sim 36^\circ$. In ZnO lattice the angle

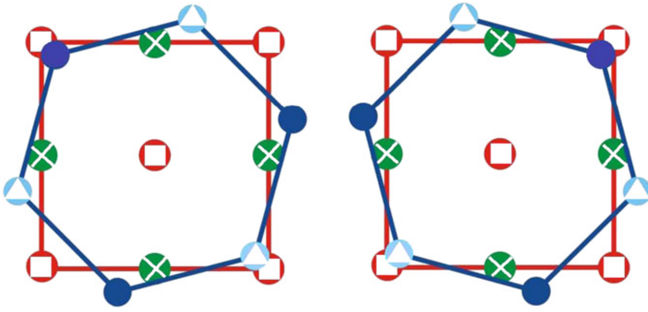

Figure 6. Schematic picture of two lattice planes—MgO (1 0 0) substrate and ZnO basal plane (0 0 0 1), each with two kinds of atoms, i.e. Mg (red circles-white squares) and O (green circles-white crosslinks) in MgO substrate and Zn (light blue circles-white triangles) and O (blue circles) in ZnO, in two probable respective rotations (lateral shifts cannot be determined from XRD).

of the (2 0 −2 5) plane with the (0 0 0 1) plane is close to 36° but no appreciable intensity at the peak position of 2 0 5 reflection could be detected in a symmetrical Bragg–Brentano scan, which can be ascribed to the very small thickness of the film. Figure 7 shows the XRD pattern measured using the grazing incidence parallel beam in the same geometry as in figure 4, but extended to higher diffraction angles. Very strong 0 0 4 reflection, which can be seen in figure 7, confirms the result of texture measurements and testifies that (0 0 0 1) planes in the ZnO film are not parallel to the (0 0 0 1) sapphire substrate but are inclined with respect to the substrate by an angle of ∼36°. The pole figure for the 1 0 1 reflection plotted in figure 5(*d*) also exhibits three-fold symmetry but the maxima are split due to the existence of domains with crystallites having slightly different orientations with respect to each other. Hence, one can conclude that the ZnO film deposited on sapphire exhibits local epitaxy, though not determined by its basal planes. Note that non-basal orientation of the ZnO film deposited on sapphire could be the reason for the lower thickness of this film, since stacking a given number of (2 0 −2 5) planes results in a lower height than stacking the same number of (0 0 0 2) planes.

Thus, ZnO films deposited on the MgO and FS substrates grow with the basal (0 0 0 1) plane parallel to the substrate. Interestingly, this is not the case for the film deposited on (0 0 0 1) sapphire, despite the fact that basal orientation, i.e. ZnO (0 0 0 1)|| sapphire (0 0 0 1), has been reported by several authors for ZnO films deposited on *c*-sapphire substrates [7, 40, 41]. The very large lattice mismatch between ZnO (0 0 0 1) and the underlying sapphire (0 0 0 1) plane is decreased after 30° in-plane rotation of the ZnO film in the basal plane leading to the epitaxial relationship of ZnO [1 0 −1 0]|| sapphire [1 1 −2 0], i.e. the *m*-plane normal direction of ZnO aligns with the *a*-plane normal of sapphire [40, 41]. However, even after the 30° in-plane rotation the lattice mismatch between ZnO and sapphire basal planes is still 18.4%, which is more than two times larger mismatch than for the MgO (1 0 0) substrate. One is led to believe that the non-basal orientation of the present ZnO film, which is evident from the XRD characterization, is related to its very small thickness. It is possible that the slightly distorted wurtzite ZnO structure with the *c*-axis inclined by ∼36° with respect to the sapphire (0 0 0 1) plane enables better matching of both lattices. The growth in the non-basal orientation is then possible only for very thin ZnO films with a high surface-to-volume ratio. From certain critical thickness the increase in the volume energy caused by distortion of the wurtzite structure prevails over the gain in the lowered interface energy with the sapphire substrate and further growth of the ZnO film takes place in the basal orientation. Further structural investigations of very thin ZnO films deposited on sapphire substrates are, therefore, highly desirable in order to fully understand this phenomenon.

The half-widths (FWHM) of the ZnO 0 0 2 rocking curves (ω-scans, not shown here) of the films on the MgO, sapphire and FS substrates were 1.2°, 1.3° and 10°, respectively. Note that the 0 0 2 rocking curve for the ZnO film deposited on the sapphire substrate was measured in asymmetric geometry with the film surface tilted by an angle of 36°. Hence, as expected, the mosaic spread of planes is relatively small for the films grown on single-crystalline substrates, while it is substantial for the film grown on the amorphous FS substrate. A comparable FWHM value of 1.15° was reported for the ZnO film on the sapphire substrate [11].

In order to determine lattice parameters of the ZnO film Θ–2Θ scans were taken for several different asymmetric reflections, i.e. with Φ and ψ angle fixed at the positions corresponding to the maximum intensity of the corresponding reflection. In the case of the film deposited on the sapphire substrate the measurement of asymmetric reflections was not efficient due to low intensity of reflections, and the lattice parameters of the film were determined using positions of the reflections in figure 7 measured in the grazing incidence geometry. The lattice parameters were determined using the LAPODS software [42] and are listed in table 1. A comparison with the values found in structure databases [43, 44] is not that trivial since there is some range of values there for both a and c. For example, in [43] records for zincite were found with $a = 0.3248$–0.3253 nm, $c = 0.5204$–0.5213 nm, if some outliers are excluded. The lattice parameters determined for the ZnO film deposited on the MgO substrate fall into the aforementioned range. The ZnO film deposited on FS and sapphire exhibits slightly higher a and shorter c lattice parameter compared with the literature [43]. However, the lattice parameters determined in ZnO films can be influenced by residual stresses induced by lattice mismatch with substrates and the stresses in the ZnO films should be, therefore, determined.

Stresses were measured by the so-called $\sin^2\psi$ method [45]. In the case of a simple biaxial stress, the measured strain σ is given by the relation

$$\varepsilon = \frac{\Delta d_{hkl}}{d_{hkl}} = \frac{1}{2}s_2\sigma\sin^2\psi + 2s_1\sigma, \qquad (2)$$

where d_{hkl} is the interplanar distance of $(h\,k\,i\,l)$ planes parallel to the sample surface and Δd_{hkl} is the change in the interplanar distance when the sample is tilted by an angle ψ. The symbols s_1, s_2 denote the x-ray elastic constants, given for elastically isotropic media as $s_1 = -(\nu/E)$; $s_2 = (1+\nu)/E$, where E and ν are the Young modulus and the Poisson ratio, respectively. The stress σ is obtained by the linear regression of $\Delta d_{hkl}/d_{hkl}$ plotted versus $\sin^2\psi$.

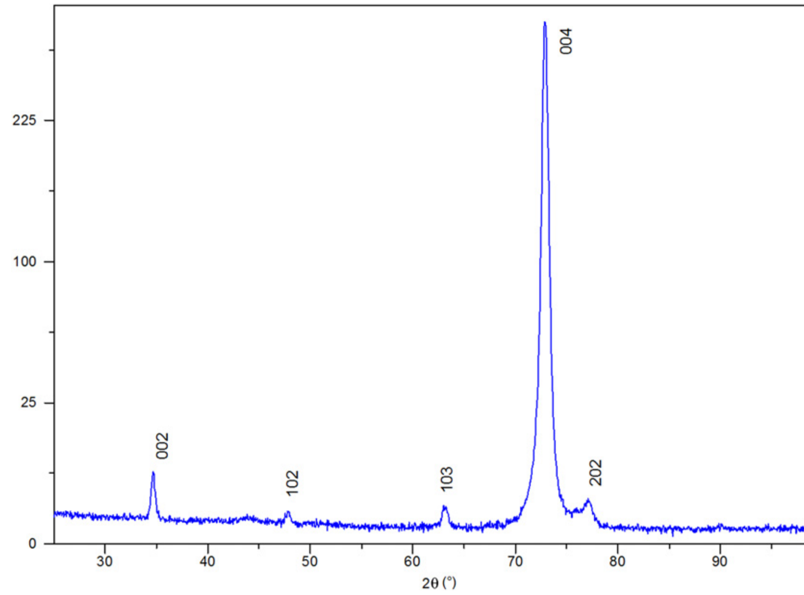

Figure 7. XRD pattern (intensity in counts per second, square-root scale) measured on the ZnO film deposited on the sapphire (0 0 0 1) substrate. The pattern was measured using the grazing incidence parallel beam with the angle of incidence $\gamma = 0.35°$.

Stress measurements in the ZnO film deposited on MgO substrate were performed for the 2 0 3, 2 1 3 and 2 0 5 reflections. An example of stress measurement at 2 0 5 reflection is shown in figure 8(*a*). Significant shifts of the peak position are clearly visible. The dependence of ε on $\sin^2\psi$ is plotted in figure 8(*b*) for the 2 1 3 and 2 0 5 reflections and presents quite linear behaviour. Data in figure 8(*b*) were analysed using equation (2) with values of the Young elastic modulus E and Poisson ratio ν of 130 GPa and 0.36, respectively [46]. This procedure yields a compressive stress of $\sigma = (14 \pm 2)$ GPa, i.e. an extremely high stress value taking into account that ZnO exhibits a hardness of 5.0 ± 0.1 GPa [47]. However, a thin ZnO film clamped on an elastically stiff substrate may be substantially harder than a free-standing bulk ZnO crystal. Indeed, it has been reported that ZnO films deposited on sapphire substrates are significantly harder than bulk ZnO crystals [48]. Although it is difficult to estimate the exact influence of both the film strong texture and the use of a narrow range of ψ values on the accuracy of the σ value, the ZnO film deposited on the MgO substrate undoubtedly suffers from high compressive in-plane stress, i.e. it is squeezed in the plane of its substrate. This is readily explained in terms of the relative lattice mismatch between cubic MgO with lattice constant $a = 4.212$ Å and wurtzite ZnO which is significant and reaches about 8%.

Stress measurements for the ZnO film deposited on the FS substrate performed on the 0 1 1 peak are shown in figure 9(*a*). The dependence of ε on $\sin^2\psi$ is plotted in figure 9(*b*) and analysis using the linear equation (2) gives a tensile stress of $\sigma = (0.90 \pm 0.13)$ GPa in the film, i.e. the film has a lattice expanded along the direction of a and contracted along the direction of c.

Stress measurements for the ZnO film deposited on sapphire were performed on the asymmetric peak 0 0 4 at various ψ inclinations. No shifts of the peak position were observed in this case, which indicates the absence of residual

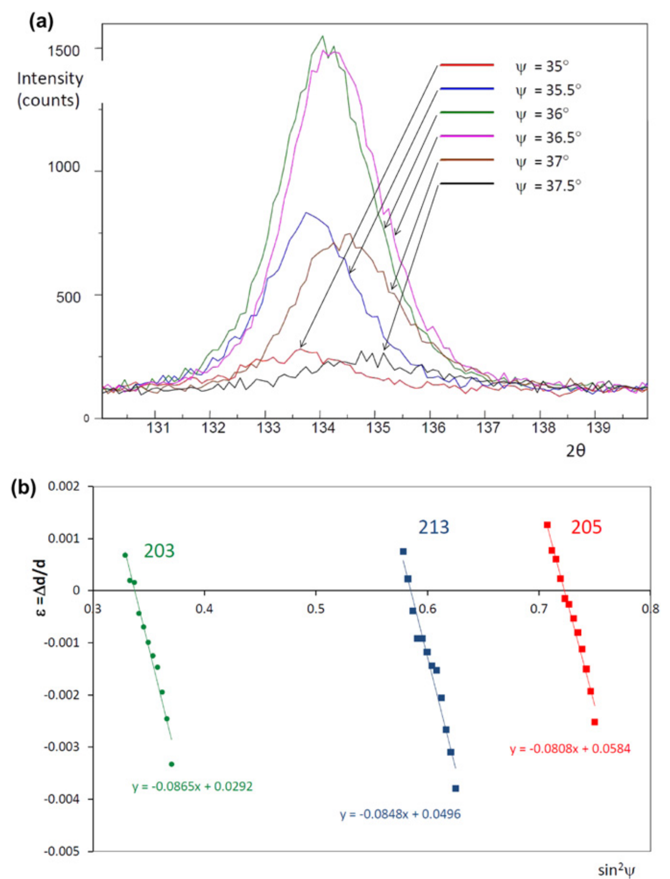

Figure 8. Stress measurements on the ZnO film deposited on the MgO substrate: (*a*) the line profile of ZnO 2 0 5 reflection for various ψ-inclinations. (*b*) Application of the $\sin^2\psi$ method to two peaks as indicated in the narrow ψ-range. Parameters of linear fits are shown. As reference stress-free d-values, the values from PDF-4+ database [44] were taken.

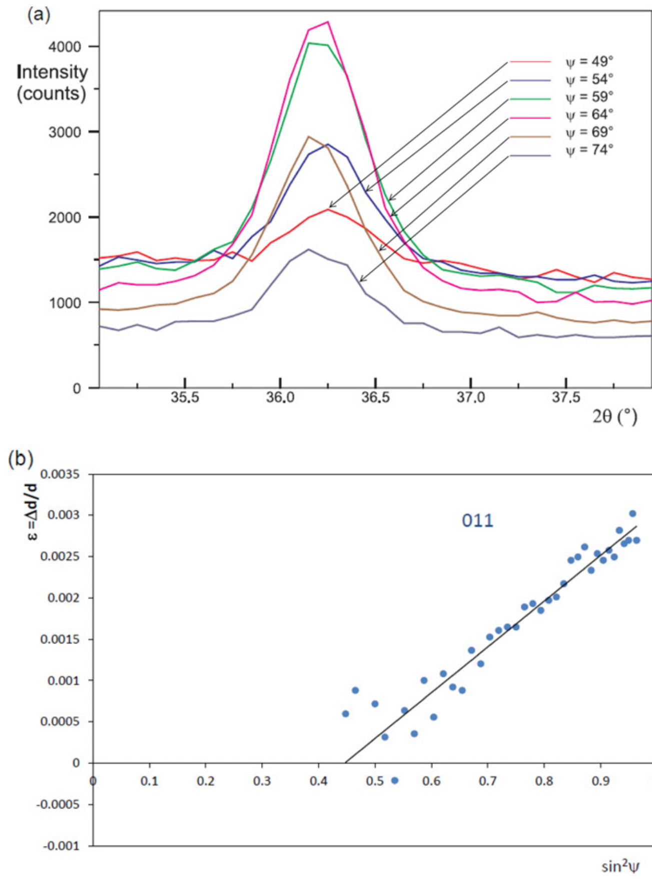

Figure 9. Stress measurements on the ZnO film deposited on the FS substrate: (*a*) the line profile of ZnO 0 1 1 reflection for various ψ-inclinations; (*b*) application of the $\sin^2\psi$ method to 0 1 1 peak in narrow ψ-range. As reference stress-free d-values, the values from PDF-4+ database [44] were taken.

stresses in the ZnO film deposited on the sapphire (0 0 0 1) substrate. This result is remarkable because the absence of residual stresses supports the picture that the non-basal orientation of the ZnO film with a slightly distorted wurtzite structure likely provides good matching with the sapphire (0 0 0 1) substrate.

All the above results of stress measurements are in full agreement with the shifts of 0 0 2 peaks observed in 2Θ scans.

3.4. Depth-resolved defects studies

The SPIS measurements were performed on (i) a reference ZnO single crystal in order to determine positron characteristics for the bulk ZnO material, (ii) bare MgO (1 0 0), sapphire (0 0 0 1) and FS substrates in order to characterize the defects in the substrates and (iii) ZnO films deposited on the MgO, sapphire and FS substrate.

The $S(E)$ curve, showing the dependence of the S parameter on the positron energy E, measured for the reference ZnO single crystal is plotted in figure 10. At the lowest energy $E = 0.03$ keV virtually all positrons annihilate on the ZnO crystal surface. With increasing energy positrons penetrate progressively deeper into the ZnO crystal and the fraction of positrons diffusing back to the surface decreases, ultimately yielding the bulk value S_0 corresponding to the

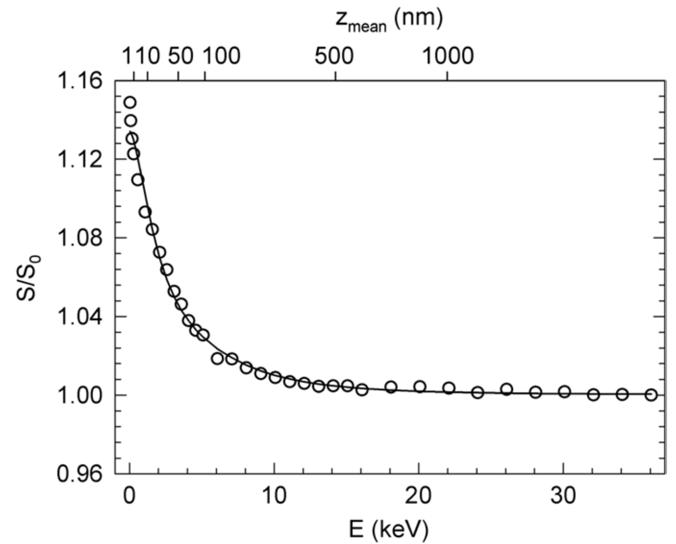

Figure 10. Reference ZnO (0 0 0 1) single crystal: dependence of the S parameter on positron energy E. The mean positron penetration depth z_{mean} is shown on the upper horizontal axis in each panel. The solid line shows the model curves calculated by VEPFIT [26].

situation when all positrons annihilate in the ZnO bulk. The $S(E)$ curve of figure 10 was fitted by the VEPFIT software package [26] using a model function calculated as a solution of the positron diffusion-annihilation equation in a single layer system. The model curve (solid line) is seen to reproduce the experimental data accurately. The mean positron diffusion length $L_0 = (47 \pm 1)$ nm obtained from fitting is in reasonable agreement with the positron diffusion length determined in a ZnO single crystal in [49]. We note that the L_0 value found for the reference ZnO crystal is significantly shorter than the mean positron diffusion length of about 100–200 nm typical for nearly defect-free semiconductors [25]. This can be explained by positron trapping in complexes consisting of Zn vacancy associated with hydrogen atoms detected in ZnO single crystals by positron lifetime spectroscopy [50].

The $S(E)$ curves for various ZnO films are plotted in figure 11. Double-layer structures assumed in the fitting of experimental points by VEPFIT [26] and consisting of ZnO film and substrate are shown in the three panels in figure 12 and compared with the experimental $S(E)$ curves. Each layer is characterized by its thickness, S parameter and the mean positron diffusion length L_+, and these are the fitting parameters in VEPFIT. The dependence of the S parameter on the positron energy can be generally written as

$$S(E) = S_{surf}F_{surf}(E) + S_{ZnO}F_{ZnO}(E) + S_{subs}F_{subs}(E), \quad (3)$$

where S_{surf}, S_{ZnO} and S_{subs} denote the S parameter and $F_{surf}(E)$, $F_{ZnO}(E)$ and $F_{subs}(E)$ denote the fractions, for positrons annihilated on the surface, inside the ZnO layer and inside the substrate, respectively. These fractions depend on the positron energy E and always satisfy the normalization condition

$$F_{surf}(E) + F_{ZnO}(E) + F_{subs}(E) = 1. \quad (4)$$

The calculated model functions plotted in figures 11 and 12 by solid lines are in satisfactory agreement with experimental points for all films.

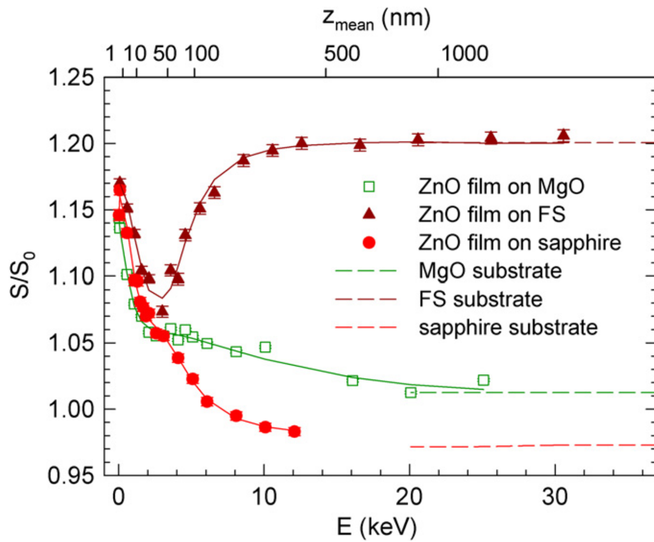

Figure 11. Results of SPIS measurements: dependence of the S parameter on positron energy E for ZnO films deposited on MgO, sapphire and FS substrates. Dashed lines show bulk S parameters measured on bare substrates. The mean positron penetration depth z_{mean} is shown on the upper horizontal axis in each panel. The solid lines show the model curves calculated by VEPFIT [26].

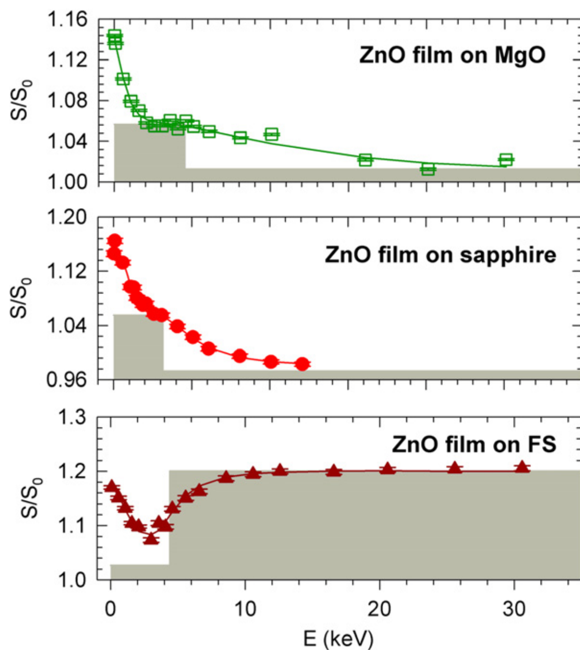

Figure 12. Layered model of ZnO films on various substrates. Each layer is represented by a box with thickness corresponding to the layer depth and height which equals the S parameter for the layer. The experimental $S(E)$ curves are plotted in the figure for comparison.

Again at the lowest energy $E = 0.03$ keV virtually all positrons annihilate on the film surface. With increasing energy positrons penetrate into the ZnO film and the fraction of positrons diffusing back to the surface decreases. Finally, positrons begin to penetrate into the substrate and S converges to the substrate value. Dashed lines in figure 11 show the S parameters, S_{subs}, determined on bare substrates. The FS substrate is characterized by a substantially higher S parameter than MgO and sapphire because fused silica exhibits lower electron density in inter-atomic regions. One can see in figure 11 that at $E > 20$ keV, the $S(E)$ curves measured on ZnO films approach the bulk values for the corresponding substrates. In order to reduce the number of fitting parameters and thereby the associated uncertainties, the positron diffusion lengths for the substrates were fixed at the values determined previously in the study of bare substrates.

The best-fit values for the S parameter, mean positron diffusion length and thickness of the ZnO layer for the various samples of this work are listed in table 1, respectively. Upon inspection of these results it becomes clear that all ZnO films have a larger value of S parameters and shorter positron diffusion length than the reference ZnO single crystal. This demonstrates that ZnO films contain concentrations of defects higher than that of the reference ZnO single crystal, independently of the substrate used in the deposition. A similar conclusion has been drawn for ZnO films deposited on sapphire and ZnO substrates by PLD [51] and by molecular beam epitaxy [52]. The ZnO films likely contain point defects similar to the reference ZnO single crystal and in addition, they will likely contain two other types of defects, namely: (i) misfit dislocations compensating the lattice mismatch between the film and the substrate and (ii) open-volume defects at grain boundaries or interfaces between various crystallites. Note that the positron diffusion length in the film deposited on the sapphire substrate is almost the same as that determined in [53] for a ZnO film deposited by PLD on the sapphire (0 0 0 1) substrate at 400 °C. ZnO films deposited on sapphire substrates at higher temperatures show progressively decreasing S parameter and increasing positron diffusion length testifying decreasing concentration of defects [53, 54].

From an inspection of the upper panel of figure 12 it becomes clear that in the film deposited on the MgO substrate the slope of the $S(E)$ curve is changed due to positrons penetrating into the MgO substrate at an energy of ≈4.5 keV corresponding to the thickness of 80 nm. The ZnO film deposited on the sapphire substrate (middle panel in figure 12) is thinner which is reflected by the change in slope of the $S(E)$ curve occurring already at an energy of ≈3.2 keV corresponding to the thickness of 45 nm. Since the positron diffusion length in the ZnO film deposited on the FS substrate is longer (see table 1) the change in the $S(E)$ curve in this film can be seen at an energy of ∼3.5 keV (lower panel in figure 12). Since the FS substrate has a higher positron affinity compared with ZnO, free positrons diffuse from the ZnO layer into the fused silica substrate. As a consequence, the $S(E)$ curve is influenced by the FS substrate already at energies lower than 4.4 keV corresponding to the film thickness of 75 nm.

The surface values of the S parameter, S_{surf}, obtained from fitting of experimental $S(E)$ curves are given in table 1. All films studied exhibit higher S_{surf} than the reference ZnO single crystal. This testifies the higher surface roughness of ZnO films compared with a high-quality bulk single crystal. The films deposited on the sapphire and FS substrates exhibit comparable surface value of the S parameter, while the film deposited on the MgO substrate exhibits a lower S_{surf} which testifies that the surface of this film is smoother.

3.5. Comparison of SPIS and XRD characterization

One can see in table 1 that the film deposited on MgO exhibits the highest S parameter and the shortest positron diffusion length among all the films studied. The S parameter measured for the ZnO film deposited on sapphire is only slightly smaller and the corresponding positron diffusion length is slightly longer. On the other hand, the film deposited on FS exhibits significantly smaller S_{ZnO} value and longer positron diffusion length. Hence, the film deposited on the MgO substrate exhibits the highest defect density, while the film deposited on the FS substrate contains the lowest concentration of defects. Hence, in general the defect densities in the films deposited on the single-crystalline substrates (MgO and sapphire) are remarkably higher than the concentration of defects in the film deposited on the FS substrate.

The XRD investigations showed that the misorientation of ZnO crystallites in the film deposited on the FS substrate is substantially higher than that in the films deposited on the single-crystalline substrates. Hence, in the ZnO film deposited on the FS substrate the mismatch between atomic positions in the substrate and in the film is, to some extent, compensated by many differing orientations (tilting) of the ZnO crystallites. As a consequence, the density of misfit dislocations in ZnO crystallites is relatively low and positrons are trapped predominantly at open-volume misfit defects at the interfaces between the crystallites. On the other hand, we have shown in the previous section that ZnO films deposited on the MgO and sapphire single-crystalline substrates exhibit local epitaxy. In these cases, the lattice mismatch between the film and the substrate is accumulated mainly by misfit dislocations. Indeed, a large number of threading dislocations was observed in the ZnO film deposited on the single-crystalline sapphire substrate by transmission electron microscopy [48]. Moreover, XRD investigations performed in section 3.3 have revealed that both films deposited on the single-crystalline substrates contain domains with different orientations. This necessarily leads to the existence of structural open-volume defects at the interfaces between these domains. Hence in the films deposited on the sapphire (0 0 0 1) and MgO (1 0 0) substrates positrons annihilated inside the crystallites are trapped at threading dislocations and positrons annihilated at the crystallite interfaces are trapped at open-volume defects there. On the other hand, in the film deposited on the FS substrate, positrons diffused to crystalline interfaces are trapped at open-volume defects, while positrons inside crystallites are annihilated from the free state. This leads to lower S parameter for the film deposited on the FS substrate although the volume fraction of crystallite interfaces in this film is higher compared with the films deposited on single-crystallite substrates due to the smaller crystallite size, see table 1.

Finally, it should be mentioned that the width of the rocking curve, which is often used for characterization of quality of epitaxial thin films, is a measure of the perfection of structural relationship but is not directly correlated with the density of defects in the film. From a comparison of XRD and SPIS results in this work we can conclude that ZnO films deposited on single-crystalline substrates (MgO and sapphire) exhibit narrow rocking curves but the net concentration of defects in these films is higher than in the film deposited on the amorphous FS substrate which is characterized by a significantly wider rocking curve.

4. Conclusions

Very thin ZnO films (thickness $\leqslant$80 nm) were fabricated by PLD on MgO (1 0 0), sapphire (0 0 0 1) and FS substrates under the same deposition conditions. Transmittance and reflectance analyses showed that the substrate plays a negligible role in the optical properties for ZnO films on MgO and FS substrates; however, we observed a slight increase in the band gap for the film on the sapphire substrate which might be attributed to the growth in non-basal orientation.

XRD investigations revealed that the ZnO layer has a wurtzite structure in all cases. The ZnO films deposited on single-crystalline substrates (MgO, sapphire) exhibit local epitaxy, while the ZnO film deposited on FS exhibits (0 0 0 1) fibre texture with random lateral orientation of crystallites in the plane of substrate. The ZnO films deposited on MgO and FS substrates grow in the basal orientation, i.e. ZnO (0 0 0 1) planes parallel to the substrate. In contrast, the ZnO film deposited on the (0 0 0 1) sapphire substrate grows in non-basal orientation with ZnO (0 0 0 1) planes inclined with respect to the substrate by an angle of $\sim$36°. Stress in ZnO films depends strongly on the substrate used. The film deposited on MgO exhibits extraordinarily high compressive in-plane stress, while the film deposited on FS exhibits tensile in-plane stress, and the film deposited on sapphire is virtually stress-free.

Depth-resolved defect studies of thin ZnO films were performed by SPIS. All the films studied exhibit higher concentrations of open-volume defects than a bulk ZnO single crystal. The ZnO films deposited on the single-crystalline substrates (MgO, sapphire) exhibits higher concentration of defects than the film deposited on the amorphous FS substrate. This can be explained by the higher density of misfit dislocations, which compensates for the lattice mismatch between the film and the substrate.

Acknowledgments

This work was supported by the Czech Science Foundation (projects GAP108/11/0958, GAP108/11/1539, GP202/09/P324)

References

[1] Kawasaki M, Ohtomo A, Ohkubo I, Koinuma H, Tang Z K, Yu P, Wang G K L, Zhang B P and Segawa Y 1998 *Mater. Sci. Eng.* B **56** 239
[2] Bagnall D M, Chen Y F, Zhu Z, Yao T, Koyama S, Shen M Y and Goto T 1997 *Appl. Phys. Lett.* **70** 2230
[3] Hu J and Gordon R G 1992 *J. Appl. Phys.* **71** 880
[4] Takahashi Y, Kanamori M, Kondoh A, Minoura H and Ohya Y 1994 *Japan. J. Appl. Phys.* **33** 6611
[5] Liu M J and Kim H K 2004 *Appl. Phys. Lett.* **84** 173
[6] Suchea M, Christoulakis S, Katharakis M, Katsarakis N and Kiriakidis G 2005 *J. Phys. Conf. Ser.* **10** 147
[7] Nie J C, Yang J Y, Piao Y, Li H, Sun Y, Xue Q M, Xiong C M, Dou R F and Tu Q Y 2008 *Appl. Phys. Lett.* **93** 173104

[8] Suchea M, Christoulakis S, Katharakis M, Kiriakidis G, Katsarakis N and Koudoumas E 2007 *Appl.Surf. Sci.* **253** 8141
[9] Villanueva Y Y, Liu D R and Cheng P T 2006 *Thin Solid Films* **501** 366
[10] Vispute R D *et al* 1997 *Appl. Phys. Lett.* **70** 2735
[11] Myoung J M, Yoon W H, Lee D H, Yun I, Bae S H and Lee S Y 2002 *Japan. J. Appl. Phys.* **41** 28
[12] Hu W S, Liu Z G, Sun J, Zhu S N, Xu Q Q, Feng D and Ji Z M 1997 *J. Phys. Chem. Solids* **58** 853
[13] Sandana V E *et al* 2009 *J. Vac. Sci. Technol.* B **27** 1678
[14] Cracium V, Elders J, Gardeniers J G E and Boyd I W 1994 *Appl. Phys. Lett.* **65** 2963
[15] Choopun S, Vispute R D, Noch W, Balsamo A, Sharma R P, Venkatesan T, Iliadis A and Look D C 1999 *Appl. Phys. Lett.* **75** 3947
[16] Özgür Ü, Alivov Y I, Lin C, Teke A, Reshchikov M A, Dogan S, Avrutin V, Cho S J and Morkoc H 2005 *J. Appl. Phys.* **98** 041301
[17] Friedrich F, Sieber I, Klaus M, Genzel C and Nickel N H 2008 *Phys. Status Solidi* c **5** 3288
[18] Schultz P J and Lynn K G 1988 *Rev. Mod. Phys.* **60** 701
[19] O'Haire R, Meaney A, McGlynn E, Henry M O, Duclère J-R and Mosnier J-P 2006 *Superlatt. Microstruct.* **39** 153
[20] Duclère J-R, Novotny M, Meaney A, O'Haire R, McGlynn E, Henry M O and Mosnier J-P 2005 *Superlatt. Microstruct.* **38** 397
[21] Anwand W, Kissener H R and Brauer G 1995 *Acta Phys. Pol.* A **88** 7
[22] Makhov A F 1960 *Fiz. Tverd. Tela (Peterburg)* **2** 2161
[23] Lynn K G and Lutz H 1980 *Phys. Rev.* B **22** 4143
[24] Mills A P and Wilson R 1982 *Phys. Rev.* A **26** 490
[25] Krause-Rehberg R and Leipner H S 1999 *Positron Annihilation in Semiconductors: Defect Studies* (Berlin: Springer)
[26] van Veen A, Schut H, Clement M, de Nijs J, Kruseman A and Ijpma M 1995 *Appl. Surf. Sci.* **85** 216
[27] Jain A, Sagar P and Mehra R M 2006 *Solid-State Electron.* **50** 1420
[28] Yakuphanoglu F, Caglar Y, Ilican S and Caglar M 2007 *Physica* B **394** 86
[29] Wang C, Chen Z, Hu H and Zhang D 2009 *Physica* B **404** 4075
[30] Look D C 2001 *Mater. Sci. Eng.* B **80** 383
[31] Pearton S J, Norton D P, Ip K, Heo Y W and Steiner T 2005 *Prog. Mater. Sci.* **50** 293
[32] Anwand W *et al* 2011 *J. Appl. Phys.* **109** 063516
[33] Muth J F, Kolbas R M, Sharma A K, Oktyabrsky S and Narayan J 1999 *J. Appl. Phys.* **85** 7884
[34] Gu Y, Kuskovsky I L, Yin M, O'Brien S and Neumark G F 2004 *Appl. Phys. Lett.* **85** 3833
[35] Djurisic A B and Leung Y H 2006 *Small* **2** 944
[36] Valerini D, Caricato A P, Lomascolo M, Romano F, Taurino A, Tunno T and Martino M 2008 *Appl. Phys.* A **93** 729
[37] Premkumar T, Manoravi P, Panigrahi B K and Baskar K 2009 *Appl. Surf. Sci.* **255** 6819
[38] Christoulakis S, Suchea M, Katharakis M, Katsarakis N, Koudoumas E and Kiriakidis G 2005 *Rev. Adv. Mater. Sci.* **10** 331
[39] Choi M H and Ma T Y 2006 *J Mater Sci* **41** 431
[40] Fons P, Iwata K, Niki S, Yamada A and Matsubara K 1999 *J. Cryst. Growth* **201–202** 627
[41] Chen Y, Bagnall D M, Koh H-J, Park K-T, Hiraga K, Zhu Z-Q and Yao T 1998 *J. Appl. Phys.* **84** 3912
[42] Dong C and Langford J I 2000 *J. Appl. Crystallogr.* **33** 1177
[43] Villars P and Cenzual K *Pearson's Crystal Data: Crystal Structure Database for Inorganic Compounds* (Materials Park, OH: ASM International®) (on CD-ROM), Release 2011/12.
[44] ICDD 2010 PDF-4+ 2010 (Database) ed Dr Soorya Kabekkodu. (Newtown Square, PA: International Centre for Diffraction Data)
[45] Noyan I C and Cohen J B 1987 *Residual Stress Measurement by Diffraction and Interpretation* (New York: Springer)
[46] Gadzhiev G C 2003 *High Temp.* **41** 778
[47] Kucheyev S O, Bradby J E, Williams J S, Jagadish C and Swain M V 2002 *Appl. Phys. Lett.* **80** 956
[48] Coleman V A, Bradby J E, Jagadish C, Munroe P, Heo Y W, Pearton S J, Norton D P, Inoue M and Yano M 2005 *Appl. Phys. Lett.* **86** 203105
[49] Koida T, Uedono A, Tsukazaki A, Sota T, Kawasaki M and Chichibu S F 2004 *Phys. Status Solidi* a **201** 2841
[50] Brauer G *et al* 2009 *Phys. Rev.* B **79** 115212
[51] Chen Z Q, Yamamoto S, Kawasuso A, Xu Y and Sekiguchi T 2005 *Appl. Surf. Sci.* **244** 377
[52] Zubiaga A, Tuomisto F and Zuñiga-Pérez J 2010 *Wide bandgap Cubic Semiconductors: From Growth to Devices* ed G Ferro and P Siffert (New York: American Institute of Physics)
[53] Honfeng R, Huimin W, Bangjiao Y, Rongdian H, Hui L and Chuanbo G 2009 *Mater. Sci. Forum* **607** 102–4
[54] Chichibu S F, Onuma T, Kubota M and Uedono A 2006 *J. Appl. Phys.* **99** 093505